Electronic Supplementary Material (ESI) for Journal of Materials Chemistry A.

Flexible and interlocked quartz fibre reinforced dual polyimide network for high-temperature thermal protection

He Huang,[a] *Xiaojie Yan,*[a] *Xiangyu Jin,*[a] *Can Wu,*[a] *Yiwu Pan,*[a] *Hebing Wang,*[a] *Chuncheng Zhu,*[b] *Changqing Hong,* [*a] *Wenbo Han,*[a] *Xinghong Zhang*[*a]

[*]Corresponding author: *hongcq@hit.edu.cn; zhangxh@hit.edu.cn*

[a]*National Key Laboratory of Science and Technology on Advanced Composites in Special Environments, Harbin Institute of Technology, Harbin, 150001, P. R. China*

[b]*Harbin Normal University, Harbin, 150001, P. R. China*

Supporting Information

1. Supplemented Figures

Table S1 The bulk shrinkage of a set of samples.

Sample ID	Original volume (cm^3)	Volume after 1st drying (cm^3)	Volume after imidization (cm^3)	Bulk shrinkage (%)
PI/QFF-P0	49.8	/	45.0	9.6
PI/QFF-P5	49.8	48.8	47.7	4.2
PI/QFF-P10	49.7	49.0	48.6	2.2

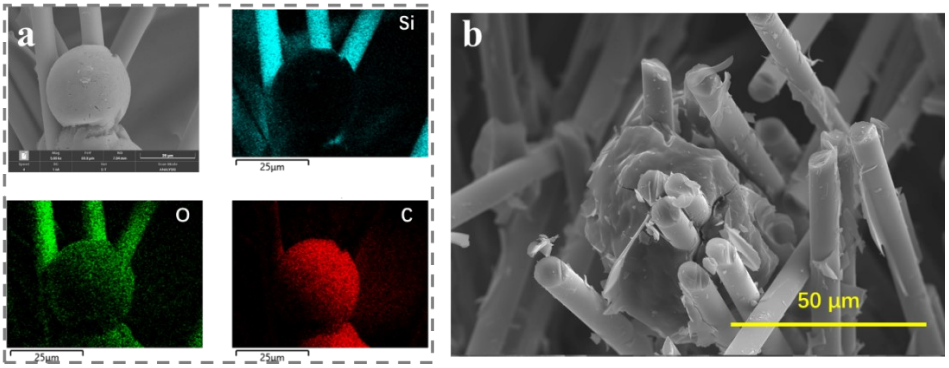

Figure S1 (a) SEM with EDS mapping images, and (b) SEM image of crossing fiber nodes bonded with linear PI and fibers coated with linear PI.

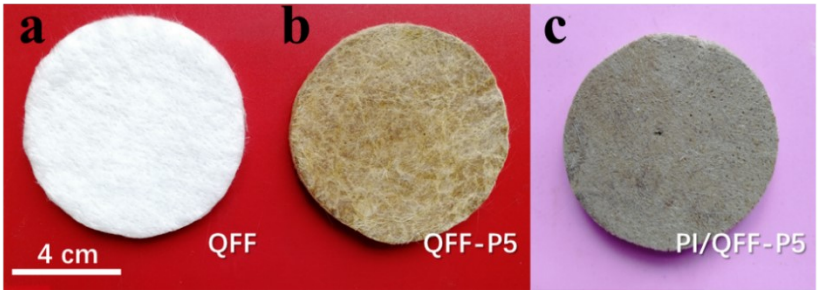

Figure S2 Photographs of the QFF (neat quartz fiber felt), QFF-P5 (polyamic acid impregnated preform), and PI/QFF-P5 (quartz fiber felt reinforced dual PI networks).

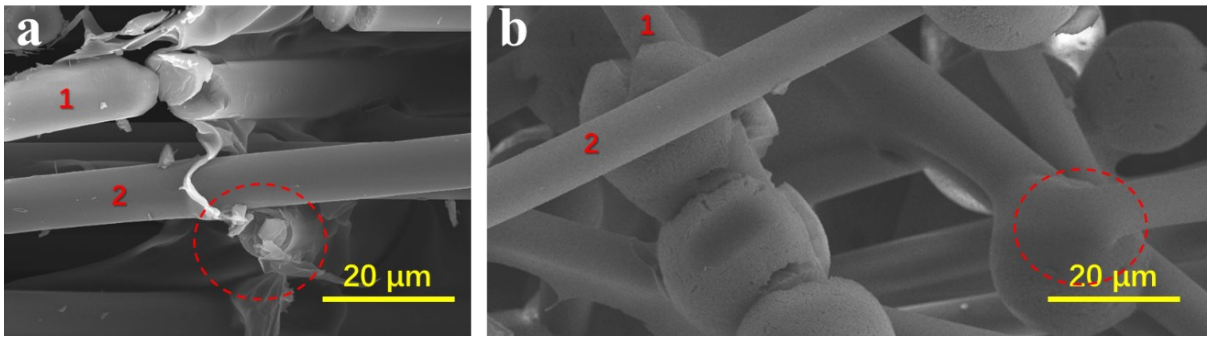

Figure S3 SEM images of PI/QFF-P0 and PI/QFF-P5 after compression test.

Discussion:

During compression or bending, the fiber is easy to break when it is crossing on another rigid fiber (Figure S3a), therefore the energy is dissipated through breaking. In Figure S3b, the fiber can be protected by the flexible buffer coating of linear PI when suffering stress during compression or bending.

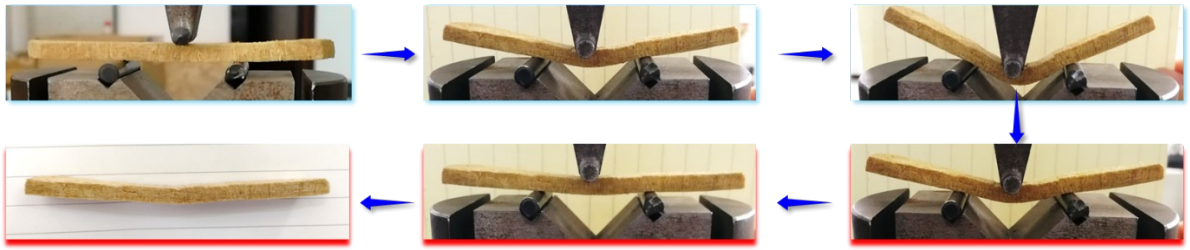

Figure S4 The images of bending process illustrating the reversible bendability of PI/QFF-P5.

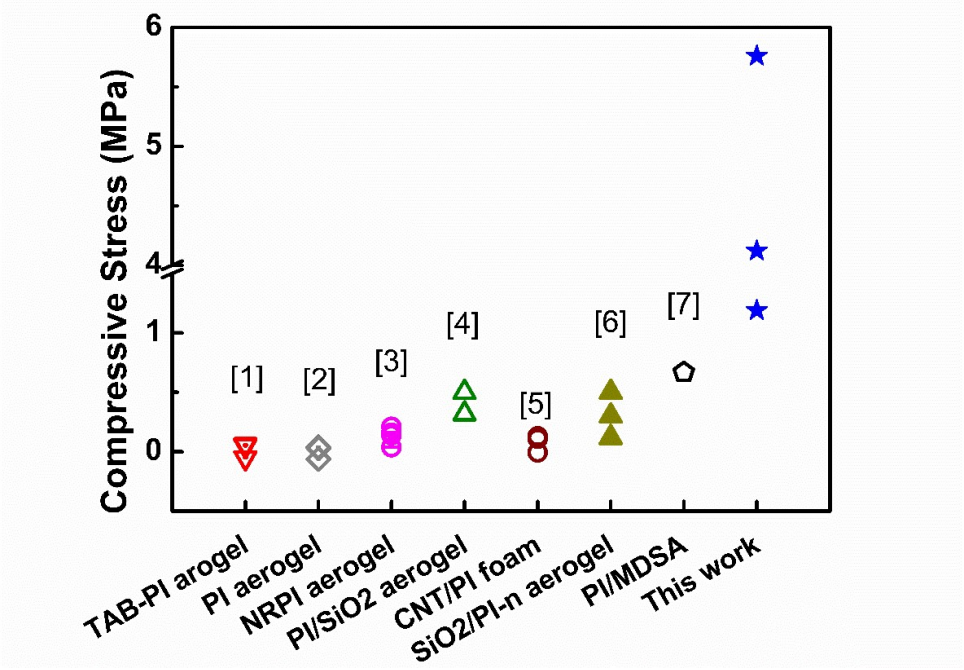

Figure S5 Benchmark of the compressive stress at 60% strain with those of flexible PI aerogels in other works.[1-7]

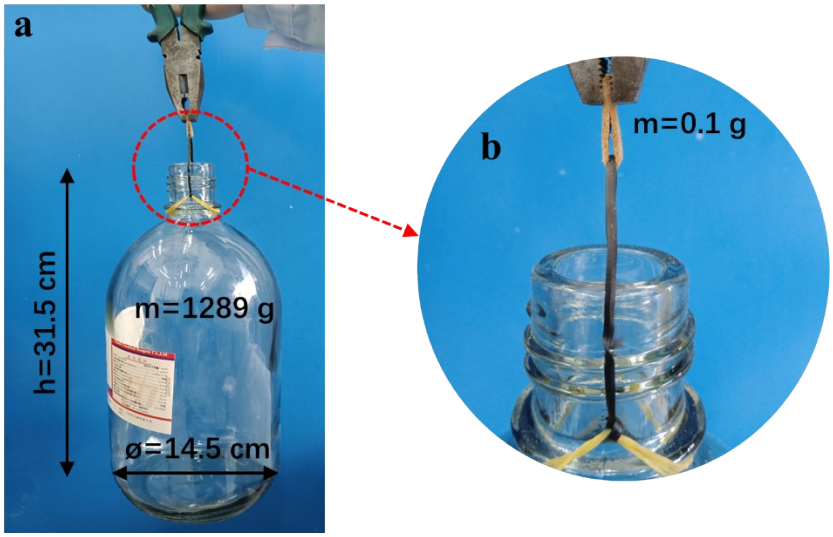

Figure S6 Photo of a 3000 mL EtOH bottle loaded on a small piece of folded PI/QFF-P5.

Figure S7 Photographs of the performance of QFF under bending and compression.

Table S2 The thermal conductivity and bulk density of a set of samples.

Sample ID	Thermal conductivity in Z ($W \cdot m^{-1}K^{-1}$)	Thermal conductivity in X/Y ($W \cdot m^{-1}K^{-1}$)	Bulk density ($g \cdot cm^{-3}$)
PI/QFF-P0	**0.038**	**0.088**	**0.147**
PI/QFF-P5	**0.036**	**0.110**	**0.204**
PI/QFF-P10	**0.039**	**0.095**	**0.252**

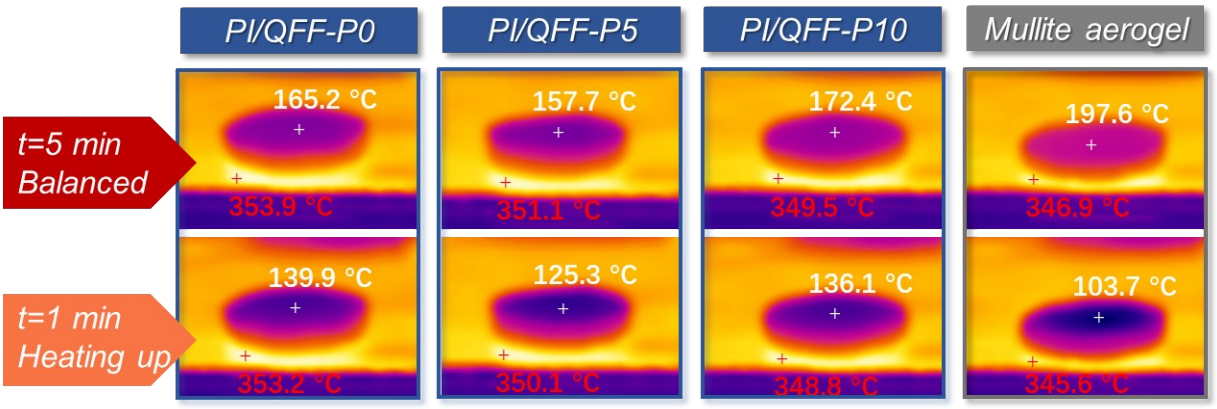

Figure S8 Thermal images of a set of samples located on a heating stage of 350 °C at the time of 1 min and 5min.

Table S3. Solid conduction λ_{sol}, interfacial thermal resistance R_K values,[8] and calculation results of PI

.

Components	λ_{sol}	R_K	D	λ^*_{sol}
	$W \cdot m^{-1}K^{-1}$	10^{-8} m^2 $K \cdot W^{-1}$	μm	$W \cdot m^{-1}K^{-1}$
PI resin	0.15–0.26	6.7–13.3	0.2	0.13–0.23

Discussion:

In the interfacial phonon scattering effect on the solid conductivity of PI, λ^*_{sol} is calculated by formula (S1):

$$\lambda^*_{sol} = \lambda_{sol}/(1 + \lambda_{sol} \times R_K/d) \quad \text{(S1)}$$

where, λ_{sol} is the thermal conductivity of equivalent solid material, R_K is the Kapitza resistance, and d is the characteristic size of the tiny pores. λ_{sol} is reduced in some extent by comparing λ^*_{sol} (0.13–0.23 $W \cdot m^{-1}K^{-1}$) with λ_{sol} (0.15–0.26 $W \cdot m^{-1}K^{-1}$) due to the phonon scattering effect. The reduced solid thermal conductivity would further decrease the solid thermal conductivity of PI/QFF-Px, based on: (1) The porous PI slice is a critical part of the crosslinked composites; (2) The PI slices are all constructed by large amounts of tiny pores, which would result in an intensive phonon scattering effect.

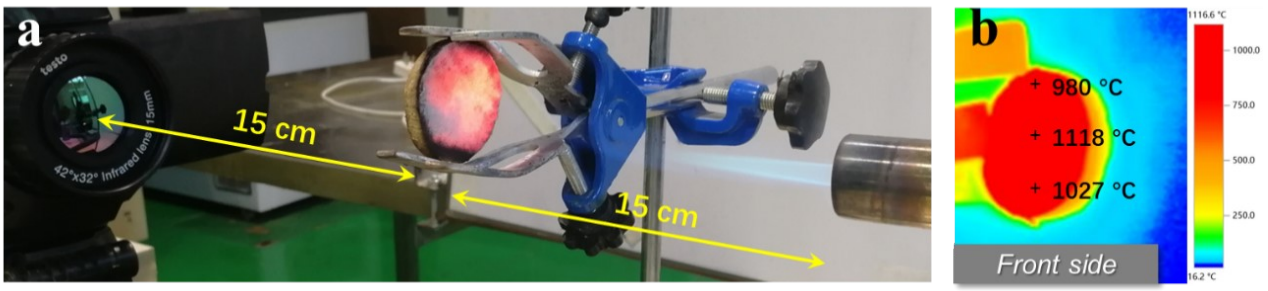

Figure S9 (a) Photographs of the measurement set-up using a butane blow torch. (b) Thermal image of the front side subjected to the butane blowlamp flame.

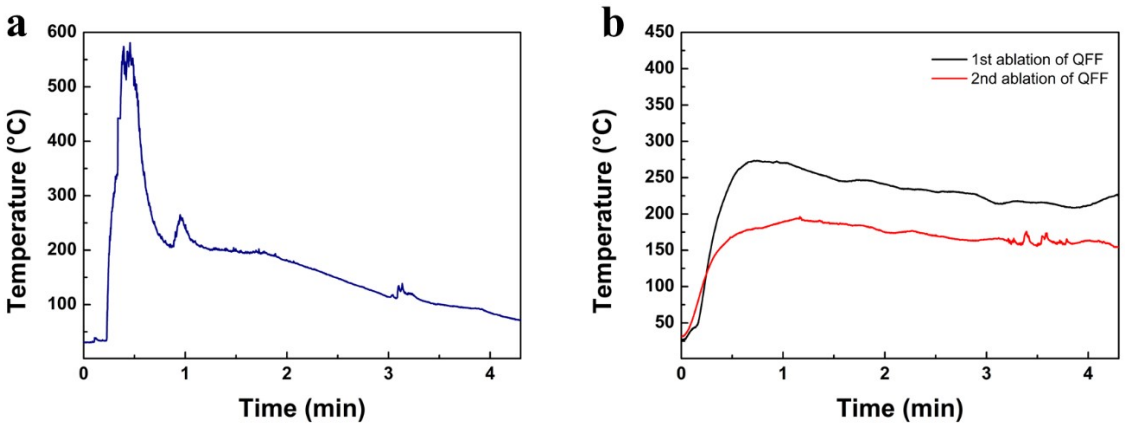

Figure S10 Backside temperature curves of (a) pure organic PI aerogel, and (b) inorganic QFF.

Discussion:

To further investigate the temperature decreases of PI/QFF-Px in stage-II, the pure organic PI aerogel and inorganic QFF were separately taken for an ablation test by being subjected to the butane flame of about 1200 °C with sufficient oxygen supply. The results of backside temperature are plotted as Fig. S9a and b, respectively. It is obvious that the temperature decrease of the composite was directly caused by the organic PI component, but not the inorganic QFF. The most significant deviation between organic aerogel and inorganic aerogels during ablation is the pyrolysis reaction, wherein both the exothermic chemical reactions and the endothermic evaporation of pyrolysis products are involved[9, 10]. Therefore, we deduce the temperature decrease in stage-IIis mainly caused by the endothermic pyrolysis of PI slices. Moreover, the marginal temperature decrease of the 1st ablation of QFF was probably caused by the organic coating on fibers, such as sizing agent. Therefore, the temperature reduction almost disappeared during the 2nd ablation of QFF as the organic component on fibers was ablated out during the 1st ablation.

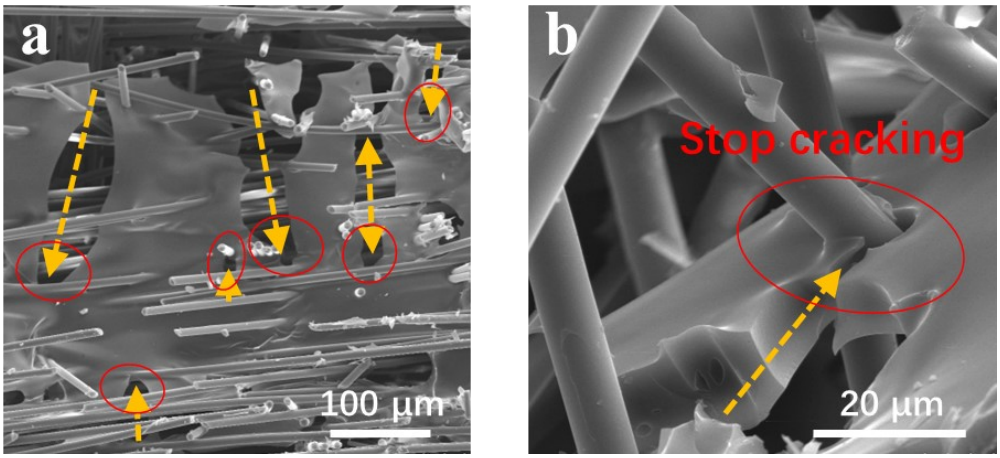

Figure S11 SEM images of the carbonized PI/QFF-P5 at different magnifications, showing the cracking stopped by fibers.

2. Supplemented Video

Video S1: Superior elasticity of PI/QFF-P0 during the repetitive compression and bending.

References

1. Y. Cheng, X. Zhang, Y. Qin, P. Dong, W. Yao, J. Matz, P. M. Ajayan, J. Shen and M. Ye, *Nat Commun*, 2021, **12**, 4092.
2. R. Yuan, Y. Zhou, X. Fan and Q. Lu, *Chem Eng J*, 2022, **433**.
3. X. Hou, Y. Mao, R. Zhang and D. Fang, *Chem Eng J*, 2021, **417**.
4. W. Fan, X. Zhang, Y. Zhang, Y. Zhang and T. Liu, *Compos Sci Technol*, 2019, **173**, 47-52.
5. Y.-Y. Wang, Z.-H. Zhou, C.-G. Zhou, W.-J. Sun, J.-F. Gao, K. Dai, D.-X. Yan and Z.-M. Li, *Acs Appl Mater Inter*, 2020, **12**, 8704-8712.
6. X. Zhang, X. Ni, C. Li, B. You and G. Sun, *Journal of Materials Chemistry A*, 2020, **8**, 9701-9712.
7. H. Huang, C. Wu, S. Wu, R. Pan, L. Yin, X. Jin, Y. Pan, H. Wang, X. Yan, C. Hong, W. Han and X. Zhang, *Chem Eng J*, 2022, **441**.
8. Z.-L. Yu, N. Yang, V. Apostolopoulou-Kalkavoura, B. Qin, Z.-Y. Ma, W.-Y. Xing, C. Qiao, L. Bergstrom, M. Antonietti and S.-H. Yu, *Angewandte Chemie-International Edition*, 2018, **57**, 4538-4542.
9. J. Yang and C. Roy, *Thermochimica Acta*, 1996, **288**, 155-168.
10. B. Ruan, H. Meng and V. Yang, *International Journal of Heat and Mass Transfer*, 2014, **69**, 455-463.